Title
Low ozone in the marine boundary layer of the tropical Pacific Ocean: Photochemical loss, chlorine atoms, and entrainment

Journal
Journal of Geophysical Research: Atmospheres, 101(D1)

ISSN
0148-0227

Authors
Singh, HB
Gregory, GL
Anderson, B
et al.

Publication Date
1996-01-20

DOI
10.1029/95jd01028

JOURNAL OF GEOPHYSICAL RESEARCH, VOL. 101, NO. D1, PAGES 1907–1917, JANUARY 20, 1996

Low ozone in the marine boundary layer of the tropical Pacific Ocean: Photochemical loss, chlorine atoms, and entrainment

H. B. Singh,[1] G. L. Gregory,[2] B. Anderson,[2] E. Browell,[2] G. W. Sachse,[2]
D. D. Davis,[3] J. Crawford,[3] J. D. Bradshaw,[3] R. Talbot,[4] D. R. Blake,[5]
D. Thornton,[6] R. Newell,[7] J. Merrill[8]

Abstract. Aircraft measurements of ozone, its key precursors, and a variety of chemical tracers were made in the troposphere of the western and central Pacific in October 1991. These data are presented and analyzed to examine the occurrence of low ozone concentrations in the remote marine boundary layer of the tropical and equatorial Pacific Ocean. The data from these flights out of Guam, covering an area extending from the equator to 20°N and from south of the Philippines to Hawaii, show average O_3 concentrations as low as 8–9 ppb (ppb = 10^{-9} v/v) at altitudes of 0.3–0.5 km in the boundary layer. Individual measurements as low as 2–5 ppb were recorded. Low O_3 concentrations do not always persist in space and time. High O_3, generally associated with the transport of upper tropospheric air, was also encountered in the boundary layer. In practically all cases, O_3 increased to values as large as 25–30 ppb within 2 km above the boundary layer top. Steady state model computations are used to suggest that these low O_3 concentrations are a result of net photochemical O_3 destruction in a low NO environment, sea surface deposition, and low net entrainment rates (3.6 ± 1.7 mm s^{-1}) from the free troposphere. Day/night measurements of select organic species (e.g., ethane, propane, C_2Cl_4) suggest that Cl atom concentrations in the vicinity of 10^5 molecules cm^{-3} may be present in the marine boundary layer in the early morning hours. This Cl atom abundance can only be rationalized if sea-salt aerosols release active chlorine (Cl_2 or HOCl) to the gas phase when exposed to sunlight. These Cl atom concentrations, however, are still insufficient, and halogen chemistry is not likely to be an important contributor to the observed low O_3.

1. Introduction

Extremely low ozone (O_3) concentrations (1–5 ppb; ppb = 10^{-9} v/v) in the boundary layer of the remote atmosphere of the tropical Pacific Ocean have been observed in a number of studies. First indications of low or undetectable O_3 levels (2 ± 2 ppb) in the marine boundary layer of the equatorial Pacific Ocean were provided by *Routhier et al.* [1980]. Low O_3 concentrations were observed in May 1978 but not in August/September 1977, suggesting that this phenomenon may not always persist in space and time. *Fishman et al.* [1987] observed 6 ppb O_3 levels in the marine boundary layer south of Hawaii (8° and 12°N) in November 1983. *Piotrowicz et al.* [1986] also made O_3 measurements in 1984 during a joint ship and aircraft research program along longitude 150°W from Hawaii (20°N) to Tahiti (17°S). Shipboard measurements (7 m) showed a distinct O_3 minimum of 8 ppb located between 4°N and 4°S. Aircraft profiles also showed that relatively high concentrations of O_3 (20–50 ppb) could be found in shallow layers trapped below the trade wind inversion. They postulated that these elevated layers originated from transport of upper tropospheric air into the marine boundary layer as well as from stratification of the boundary layer under low wind speed (nighttime) conditions. Based on data obtained during a cruise from Central America to American Samoa (15°S, 170°W) in January/February 1990 and from a 10-year record of O_3 observations at Samoa, *Piotrowicz et al.* [1991] concluded that synoptic-scale atmospheric circulation was an important determinant of equatorial Pacific O_3 data. In all of these experiments the focus was on O_3 and few other chemical precursor species were measured. The mechanism by which these low concentrations are sustained is not known although both transport and photochemical schemes have been proposed [*Chameides and Davis*, 1980; *Liu et al.*, 1983; *Newell and Wu*, 1985; *Piotrowicz et al.*, 1991].

The Pacific Exploratory Mission (PEM)-West A airborne expedition of September/October 1991 provided an opportunity to study these low O_3 levels in the western tropical Pacific in greater chemical detail. This was the first time that virtually all possible O_3 precursors (reactive nitrogen species, CO, C_1-C_7 hydrocarbons, halocarbons, gaseous and aerosol Cl, sulfur species, and peroxides) were measured simultaneously, providing the possibility of a mechanistic understanding of

[1]NASA Ames Research Center, Moffett Field, California.
[2]NASA Langley Research Center, Hampton, Virginia.
[3]Georgia Institute of Technology, Atlanta.
[4]University of New Hampshire, Durham.
[5]University of California, Irvine.
[6]Drexel University, Pennsylvania.
[7]MIT, Cambridge, Massachusetts.
[8]University of Rhode Island, Narragansett.

Paper number 95JD01028.
0148-0227/96/95JD-01028$05.00

Table 1. Ozone Measurements in the Marine Boundary Layer of the Tropical Pacific Ocean Obtained During PEM-West A

Mission	October 1991	Departure Point	Time Period, UT	Latitude, °N	Longitude	Altitude, km	Ozone, ppb	Ozone, ppb, Range	Static T_{air}, °C	Radiometric T_{sea}, °C	Relative Humidity %
15	11	Guam	0330:30–0421:30	−0.06–0.41	158.57°–161.57°E	0.34 ± 0.00	8.8 ± 1.4 275*	2.4–11.9	26.5	29.5	73.0
16	13	Guam	0413:30–0454:30	4.17–5.15	124.88°–127.62°E	0.34 ± 0.00	8.4 ± 1.7 209	5.1–13.9	26.4	29.5	72.1
17	14–15	Guam	1934:30–2005:30	14.66–15.10	139.58°–141.95°E	0.48 ± 0.00	13.0 ± 2.0 186	8.0–18.1	24.9	28.7	80.9
			2127:30–2211:30	14.80–15.00	139.00°–142.00°E	0.40 ± 0.00	14.8 ± 2.6 264	8.1–20.9	25.4	28.8	81.0
			2310:30–2330:30	15.00–15.03	140.50°–142.08°E	0.41 ± 0.00	12.4 ± 1.6 120	7.6–16.4	25.5	28.8	77.7
			0050:30–0119:30	14.98–15.05	139.07°–141.43°E	0.40 ± 0.00	14.2 ± 2.5 174	8.7–23.9	25.7	28.9	79.5
18	18	Guam–Wake Island	0138:30–0212:30	12.90–13.01	158.21°–161.30°E	0.36 ± 0.00	8.5 ± 1.5 204	4.3–12.7	25.0	29.5	82.7
19	19	Wake Island–Hawaii	0016:30–0048:30	15.09–16.58	178.64°–176.83°W	0.36 ± 0.00	38.0 ± 2.0 192	32.9–42.4	24.0	28.3	76.9
20	20	Hawaii	1449:30–1534:30	18.73–20.78	155.69°–154.32°W	0.49 ± 0.01	21.8 ± 2.1 270	17.0–26.7	20.5	26.7	87.1
			1818:30–1846:30	18.52–19.28	155.61°–154.71°W	0.38 ± 0.00	21.4 ± 1.8 168	16.8–25.4	21.5	26.8	85.6

*Mean ±1 standard deviation, number of data points.

factors that could explain the existence of low O_3 values in the tropical boundary layer. Instrumentation aboard the NASA DC-8 aircraft and the basic flight plans are summarized in the overview paper by *Hoell et al.* [this issue]. Results from the airborne differential absorption lidar (DIAL) and the background meteorology of the western Pacific are described by *Browell et al.* [this issue] and *Bachmeier et al.* [this issue], respectively. This paper describes aircraft measurements of ozone as well as important precursor and chemical tracers in the marine boundary layer of the tropical and equatorial Pacific Ocean from south of the Philippines to Hawaii and between the equator and 20°N. The O_3 data are related to other chemical in situ aircraft measurements, to characteristic boundary layer features in the vertical temperature and humidity profiles, and to concurrent lidar data. Photochemical and meteorological calculations are used to suggest a scenario in which low net entrainment rates and high photochemical loss rates, resulting from extremely low NO levels, are adequate to maintain the observed O_3 abundances.

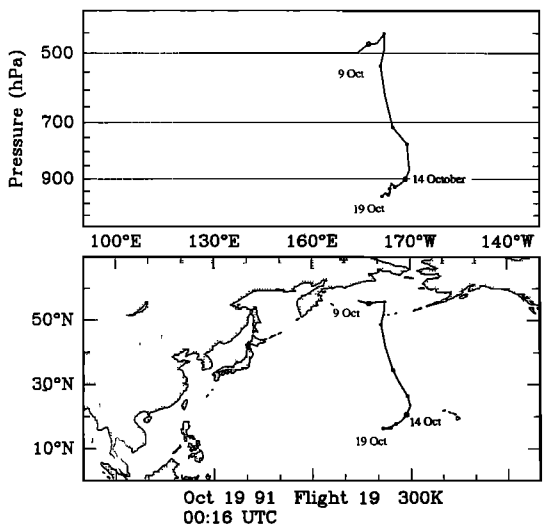

Figure 1a. Ten-day isentropic (300 K) three-dimensional air parcel back trajectory relevant to the high O_3 concentrations measured in the marine boundary layer of the tropical Pacific Ocean between Wake Island and Hawaii during PEM-West A mission 19 (October 19, 1991, 0016 UT). Top and bottom panels show vertical and horizontal path projection, respectively.

2. Analysis of Measurements

Boundary Layer

Table 1 summarizes the PEM-West A missions that provided the low-altitude O_3 measurements in the tropical Pacific

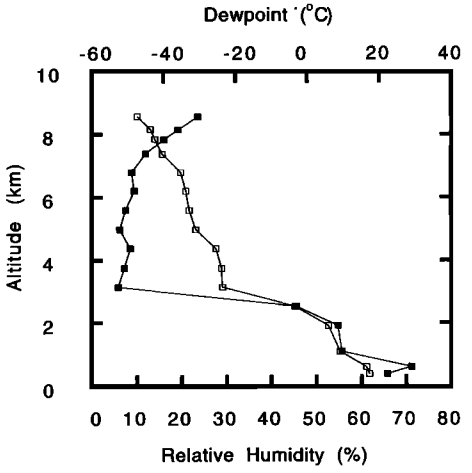

Figure 1b. Vertical profile of relative humidity (solid square) and dew point (open square) obtained by aircraft on its descent to the boundary layer during mission 19 (2351:30–0016:30 UT). Dry air above 2 km is characteristic of descending air parcel trajectory of Figure 1a.

Ocean. The NASA DC-8 made horizontal flights of about 30- to 50-min duration at altitudes that varied from 340 to 490 m above sea level. Vertical profiles of O_3 concentrations as well as ambient air temperature and humidity were obtained during the aircraft descent to and the climb from the low-altitude flight leg. On missions (M) 15, 16, 17, and 18 the airplane departed Guam, respectively, southeastward to the equator (M15), westward to south of the Philippines (M16), to 800 km west of Guam (M17), and toward Wake Island (M18). During M19 the plane flew from Wake Island to Hawaii, and on M20, low-altitude measurements were made around the Hawaiian islands. Table 1 lists the O_3 concentrations (means, standard deviations, number of measurements) and their ranges for each low-altitude pass. Values ≤5 ppb were measured on M15, M16, and M18. Mean concentrations for these missions were

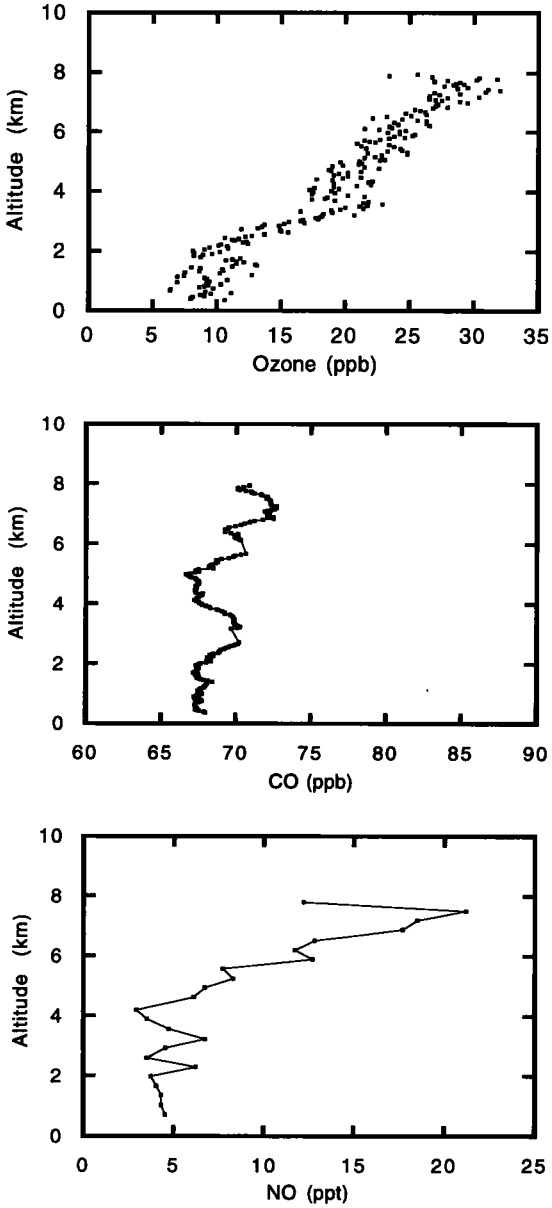

Figure 2. Vertical profiles of O_3, CO, and NO obtained in the tropical Pacific Ocean near 0.4°N and 161.6°E during PEM-West A mission 15 (October 10/11, 1991, 0253:30–0329:30 UT).

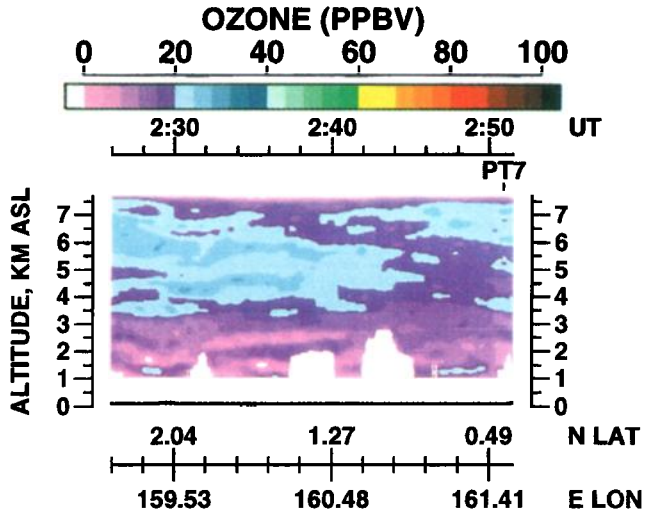

Figure 3. Horizontal and vertical distribution of O_3 measurements from the downward looking differential absorption lidar (DIAL) obtained at 0230–0250 UT during mission 15. Low O_3 concentrations (<10 ppb) are observed at and below 2.5 km. Lidar observations show large spatial variations in the vertical and horizontal O_3 distribution.

8–9 ppb. These, however, were somewhat higher for M17 (12–15 ppb) and significantly higher for M19 (38 ppb). These relative differences appear to be related to the differences in the air mass source region as indicated by the isentropic air parcel trajectories computed by *Merrill* [this issue]. For M15, M16, and M18 both high- and low-altitude trajectories indicated that the sampled air parcels originated and remained over the tropical Pacific for a period of 5–10 days prior to their sampling. On the other hand, for M17, when higher concentrations of O_3 were measured west of Guam, air parcels originated from the Asian continent. During M19 a deep 500-mbar low-pressure trough extended from Alaska to latitude 15°N along longitude 170°W–180°. Figure 1a shows a 10-day isentropic trajectory relevant to the low-altitude aircraft flight of M19 (0016:30–0048:30 UT). The bottom panel traces the air parcel (located at 18°N 180° longitude, 970 mbar or 360 m, at 0016 UT) to the outer Aleutian Islands about 10 days earlier. The top panel shows that the air parcel descended from 500 mbar (5.6 km) to 970 mbar (0.36 km) during that time period. Figure 1b shows the vertical profile of humidity (90-s data) obtained by the aircraft on its descent to the boundary layer (2351:30 to 0016:30 UT). The dry air above 2 km is compatible with the long descending air parcel trajectory shown in the top panel of Figure 1a. It is therefore evident that the boundary layer air sampled during M19 at 15°–16°N between Wake Island and Hawaii was directly affected by transport from a high-altitude northern latitude area of high O_3. In fact, PEM-West A obtained a vertical profile of O_3 over the outer Aleutian Islands during mission 5 on September 17–18, 1991. The profile showed O_3 concentrations of 46 ppb at 5.6 km. This high-O_3 transport into the marine boundary layer is in accordance with the findings by *Piotrowicz et al.* [1991] for the tropical Pacific Ocean and by *Paluch et al.* [1994] for the subtropical marine boundary layer of the eastern Pacific Ocean. The O_3 concentrations around the Hawaiian islands during M20 (mean values of 21–22 ppb with a range of 16–26 ppb) were similar to those measured by *Piotrowicz et al.* [1986] during the summer and fall seasons of 1984 (20–30 ppb).

Table 2. Air Concentrations of Precursors and Relevant Chemical Species Measured Concurrently With Low O_3 Concentrations in the Marine Boundary Layer of the Tropical Pacific Ocean During PEM-West A

Time, UT*	Mission	Altitude, km msl	Ozone, ppb	CO, ppb	NO, ppt	NO_2, ppt	NO_y, ppt	HNO_3, ppt	PAN, ppt	C_2Cl_4, ppt
0330:30–0421:30	15	0.34±0.00	8.8±1.4 275†	67.7±0.5 267	5.0±1.0 19	17.0±2.5 19	···	19.0±11.1 4	2.4±1.0 6	2.2±0.4 6
0413:30–0454:30	16	0.34±0.00	8.4±1.7 209	91.7±3.4 206	9.6±7.1 20	15.7±3.1 20	323.0±36.5 20	16.0±7.0 3	2.0±0.0 5	2.1±0.3 5
1934:30–2005:30(N)	17	0.48±0.00	13.0±2.0 186	118.3±2.3 160	3.7±0.3 15	15.0±5.0 15	···	29.5±2.1 2	2.0±0.0 4	2.2±0.6 4
2127:30–2211:30	17	0.40±0.00	14.8±2.6 264	116.7±1.5 234	5.1±4.1 21	16.5±10.6 21	···	16.7±7.5 3	2.0±0.0 4	2.4±0.7 4
2310:30–2330:30	17	0.41±0.00	12.4±1.6 120	115.4±2.1 94	6.8±2.6 8	19.3±6.1 8	143.1±22.3 8	···	2.0±0.0 3	2.0±0.2 3
0050:30–0119:30	17	0.40±0.00	14.2±2.5 174	115.1±2.3 150	4.6±2.1 10	14.1±1.5 10	154.9±27.8 10	14.0±9.9 2	2.0±0.0 3	2.3±0.8 3
0138:30–0212:30	18	0.36±0.00	8.5±1.5 204	72.6±0.5 177	3.6±1.0 14	14.8±2.6 3	173.5±19.8 14	···	2.0±0.0 4	2.8±0.9 4
0016:30–0048:30	19	0.36±0.00	38.0±2.0 192	97.9±3.6 159	3.1±0.6 12	12.4±1.4 12	518.1±90.7 12	14.5±2.1 2	2.9±1.6 3	5.2±0.6 3
1449:30–1534:30(N)	20	0.49±0.01	21.8±2.1 270	75.7±1.3 214	1.9±0.3 21	15.1±20.7 21	109.6±30.6 21	21.5±2.1 2	2.9±2.0 5	4.2±1.0 5
1818:30–1846:30	20	0.38±0.00	21.4±1.8 168	74.9±1.1 145	2.9±1.4 14	11.3±1.5 14	83.3±13.8 14	···	2.0±0.0 4	3.7±0.4 4

Time, UT*	Mission	C_2H_6, ppt	C_2H_4, ppt	C_2H_2, ppt	C_3H_8, ppt	C_3H_6, ppt	Benzene, ppt	SO_2, ppt	DMS, ppt	H_2O_2, ppt
0330:30–0421:30	15	369.5±13.4 2	18.0±8.5 2	17.5±2.1 2	11.5±0.7 2	9.5±5.0 2	8.0±1.4 2	38.7±6.6 7	46.1±12.8 7	584.4±90.3 207
0413:30–0454:30	16	461.3±13.6 3	21.0±12.1 3	56.7±8.5 3	19.3±7.4 3	···	27.0±0.0 2	62.2±18.4 6	25.5±4.6 6	1630.5±101.1 182
1934:30–2005:30(N)	17	653.7±21.5 3	21.7±4.5 3	123.0±2.0 3	39.0±2.7 3	11.3±4.0 3	51.0±15.7 3	40.2±8.4 5	20.8±1.9 5	···
2127:30–2211:30	17	630.7±33.3 3	11.7±0.6 3	120.0±15.5 3	39.3±2.5 3	···	40.7±6.0 3	40.9±5.3 7	25.4±2.5 7	1653.3±93.5 183
2310:30–2330:30	17	628.7±28.7 3	11.0±4.0 3	87.7±7.1 3	32.0±2.7 3	···	32.5±2.1 2	59.0±17.7 3	23.3±6.0 3	1618.1±116.9 120
0050:30–0119:30	17	629.0±0.0 1	13.0±0.0 1	···	36.0±2.8 2	···	37.0±0.0 1	40.3±6.8 3	22.0±7.1 2	2092.6±102.2 64
0138:30–0212:30	18	371.3±21.6 3	26.3±7.8 3	28.7±10.0 3	16.0±9.5 3	13.3±2.9 3	12.0±4.0 3	29.7±1.9 6	33.3±2.7 6	519.5±79.1 81
0016:30–0048:30	19	1102.0±92.9 4	25.0±8.1 4	···	195.8±40.0 4	15.3±5.4 4	42.5±12.8 4	40.4±11.2 5	17.4±5.7 5	1372.9±260.3 150
1449:30–1534:30(N)	20	570.0±26.9 7	13.9±5.4 7	63.3±10.4 7	49.1±8.9 7	10.5±2.1 2	14.9±5.4 7	74.1±103.8 7	21.4±2.9 7	932.6±97.5 205
1818:30–1846:30	20	549.5±34.7 2	14.0±4.2 2	55.5±10.6 2	42.0±2.8 2	···	14.0±1.4 2	30.8±4.6 4	25.5±1.0 4	851.5±70.5 104

*N indicates nighttime; all other data are collected during daytime.

†Mean ±one standard deviation, number of data points. Ozone and CO are 10-s data; HNO_3 is as measured, all other data are taken from a merged file based on the 3-min NO_y time window.

Table 2 lists the measured mean concentration of O_3 together with that recorded concurrently for various precursors (i.e., NO_x, CO, C_1-C_7 hydrocarbons) and other relevant chemical species. Standard deviations and the total number of measurements are also indicated. All data presented in Table 2 were derived from merged files as noted. Concentrations of reactive nitrogen species (NO, NO_2, HNO_3, and PAN) were extremely low and, as we shall see below, inhibited ozone production. It is likely that much of the available NO_x is oxidized to HNO_3 and deposited on the ocean surface. CO concentrations, an indicator of pollution, ranged from about 67 ppb (M15) to 118 ppb (M17). These average values are similar to those measured in the boundary layer in Alaska (70–80 ppb) and Labrador (103–107 ppb) during ABLE 3B [*Singh et al.*, 1994]. The relatively high CO concentrations measured during M17 (115–118 ppb) can again be related to air parcel trajectories from the Asian continent and are therefore indicative of an anthropogenic (polluted) impact on the tropical lower marine boundary layer west of Guam. A select group of C_1-C_7 hydrocarbons show low concentrations similar to those obtained from shipboard measurements in the equatorial eastern Pacific Ocean and the southern hemisphere by *Singh et al.* [1988]. Similarly, dimethyl sulfide (DMS) and SO_2 levels were typical of tropical waters of low biological activity and were not correlated with the O_3 present.

Vertical Profiles

Mission 15. Figure 2 shows the vertical distribution of O_3, CO, and NO obtained on M15 (Guam to equator) when the aircraft descended from about 8 km to the boundary layer during a 36-min period and over a horizontal distance of not more than 35 km. Low O_3 and CO concentrations extended

from 340 to 2000 m but then increased rapidly with altitude to 22 and 70 ppb, respectively, at 3.0–3.5 km. Above 3.5 km, O_3 continued to increase steadily to 30 ppb at 8 km while CO increased through a multilayered structure to more than 70 ppb at 7 km. The vertical NO profile shows very low concentrations (around 5 ppt) up to 4 km but then increases to 20 ppt at 7.5 km. Thus all three species were more abundant in the free troposphere than in the boundary layer. The vertical temperature profile obtained by the descending aircraft showed a stable layer (not an inversion) at 2.0 km and a second stable layer from about 3.0 to 3.5 km. These stable layers correspond to the large changes in O_3 with altitude shown in the vertical profile of Figure 2 and also to the layered structure of CO and NO.

For M15, O_3 measurements from the downward looking lidar system were available from about 0230–0250 UT just before the aircraft started its descent to the marine boundary layer (Figure 3). Between 0230 and 0240 UT, low O_3 concentrations (<10 ppb) were observed at and below 2.5 km. Concentrations increase to >20 ppb above 3.0 km. This crossection of lidar data therefore is similar to the vertical O_3 profile of Figure 2. The lidar data, however, show large spatial variations in the vertical and horizontal O_3 distribution. No aerosol distribution data were available to identify the mixing layer or the top of the boundary layer. Figure 3 also presents evidence of the presence of cumulus clouds below the 2.0- to 2.5-km level at three different locations.

Mission 18. Figure 4 shows the altitude profiles of O_3, CO, NO, and relative humidity (90-s data) observed during M18 (Guam to Wake Island) when the DC-8 climbed from the boundary layer to 10 km altitude during a time period of 30 min and over a horizontal distance of about 200 km. O_3 concentrations were less than 10 ppb in the shallow 1000-m boundary layer but then increased sharply to more than 30 ppb at about 3 km altitude. At the same time, CO concentrations increased from 72 to 86 ppb and relative humidity decreased from 85 to 60%. These changes are much greater than those encountered during mission 15 (Figure 2). The vertical temperature profile showed a stable layer from 1.0 to 1.5 km and a second very narrow stable layer at 3 km altitude. Above 3 km, O_3 values remain at 24–30 ppb with large spatial variability, while CO concentrations vary from 78 to 82 ppb with multilayered structure. NO values were very low up to 7.5 km and then increased rapidly to about 9 ppt in the upper troposphere.

The O_3 distributions observed by the upward looking DIAL during the low-level pass of the aircraft through the marine boundary layer (not shown) were limited to altitudes above 3 km. The lidar indicated O_3 concentrations of 25–30 ppb from 3 to 8 km with spatial variability similar to that shown in the vertical O_3 profile of Figure 4. Patchy concentrations less than 20 ppb, not seen in the vertical profile of Figure 4, were observed above 6 km. The lidar-observed aerosol distributions, starting at 1 km altitude, showed dense aerosol plumes or clouds with tops at 1.5–2.0 km and thus support the existence of the shallow mixing layer indicated in Figure 4 by low O_3, CO, and NO concentrations and high relative humidity.

Mission 16. Figure 5 shows the vertical profiles of O_3, CO, NO, and relative humidity obtained during M16 south of the Philippines when the DC-8 descended to the marine boundary layer. In addition to low (<10 ppb) O_3 concentrations at 340 m, an elevated layer of relatively high O_3 (20–25 ppb) and CO (140–160 ppb) is shown. This layer is identified in the relative humidity profile by a decrease in humidity from 75 to 40%. It appears to be a pollution plume because of the high CO. NO concentrations remained low. However, isentropic trajectories computed by *Merrill* [1994] at 950 mbar (500 m) were easterly, and also, winds from the aircraft inertial navigation system were northeast to east and therefore gave no direct indication of possible transport from the Philippines to the north or from Borneo to the west.

Figure 6 presents the O_3 and aerosol distributions obtained from the downward looking DIAL from 0250 to 0330 UT just before the aircraft's descent to the boundary layer. The elevated O_3 layer (>20 ppb) is seen at 1.5–2.0 km and coincides with a layer of large aerosol backscatter above the mixing layer which, in the lidar data, extends from sea level to 1 km. Thus the remote lidar data are in agreement with the in situ O_3 measurements displayed in Figure 5. Again a lot of spatial variability is detected in both the aerosol and the O_3 data. Scattered clouds were present in the lidar aerosol cross section at 4 and 6 km. The temperature and humidity profiles showed a moist (75%) marine boundary layer from sea level to 0.5–1.0 km with a dry (43%) stable layer above. Most likely, the observed pollution plume arrived at the 1.5- to 2.0-km level from some distant pollution source by downward transport judging from the dryness of the layer. The plume could then be advected by the horizontal wind field over a large distance.

Day/Night Measurements

Daytime and nighttime measurements of O_3, ozone precursors, and other chemical species in the marine boundary layer were made during M17 and M20, as noted in Table 2. The motive was to test any fast radical chemistry, especially Cl chemistry, that may occur in a short period of 2–3 hours. Some gaseous and aerosol halogen species were also measured by ion chromatographic analysis. Gaseous species were sampled using the mist chamber technique and aerosols by filter collection [*Talbot et al.*, 1990]. It is pointed out that while a substantial fraction of gaseous Cl is probably HCl, other molecules such as Cl_2 or HOCl may also be nonspecifically included. Table 3 lists the measured daytime and nighttime concentrations of gaseous Cl, aerosol Cl, and aerosol sodium (Na). On the average, Cl/Na ratios measured were quite low and substantial degassification appears to have already occurred [*Singh*, 1995]. The gaseous Cl shows a slight increase from 25–32 ppt at night to 31–49 ppt during daytime in the marine environment of M17 and a somewhat larger increase from 111–123 ppt at night to 156–240 ppt during the day over Hawaii (M20). As expected, the Cl/Na ratio decreased for both M17 and M20 qualitatively in line with increasing gaseous Cl, suggesting degassing of aerosol Cl.

3. Discussion and Results

To understand the low O_3 concentrations in the marine boundary layer, a simple steady state box model concept was employed. In this model, O_3 in the boundary layer is maintained by entrainment of free-tropospheric O_3 across the top (net entrainment velocity V_e), deposition at the sea surface boundary (deposition velocity V_d), and the net O_3 photochemical tendency $P(O_3)$. For such a system to be in balance,

$$V_e = \{[O_3\ (T_s,\ P_s)]_{bl} V_d - h_{bl} P(O_3)\}/\{[O_3\ (T_f,\ P_f)]_{ft} - [O_3\ (T_{tbl},\ P_{tbl})]_{bl}\} \quad (1)$$

where h_{bl} is the height of the boundary layer and $[O_3]_{bl}$ and $[O_3]_{ft}$ are ozone concentrations in the boundary layer and the

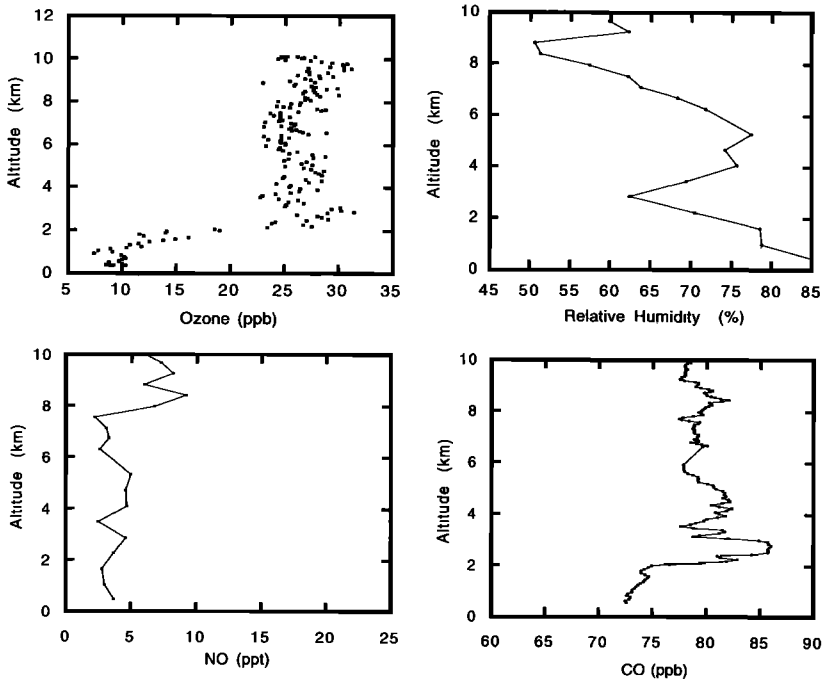

Figure 4. Vertical profiles of O_3, CO, NO, and relative humidity obtained in the tropical Pacific Ocean near 13.0°N and 161.4°–164.3°E during PEM-West A mission 18 (October 17/18, 1991, 0212:30–0242:30 UT).

free troposphere, respectively. Since concentrations expressed in molecules per cubic centimeters are a function of temperature and pressure, these are noted in (1). Subscripts *s*, *tbl*, and *f* represent conditions just above the sea surface, below the top of the boundary layer, and the free troposphere (above the boundary layer), respectively. This simplified model assumes that horizontal transport is not important in this region. Independent meteorological analysis was performed to see if V_e calculated from (1) was reasonable for the prevailing conditions. If meteorological analysis and literature suggest that the expected net entrainment rates should be much higher than calculated, then additional loss mechanisms in the boundary layer would be required to explain the low-O_3 observations. Free-tropospheric O_3 concentrations were obtained from the measured vertical O_3 profiles (such as Figures 2 and 4). The surface deposition rate was assumed to be 0.26 mm s^{-1}, the

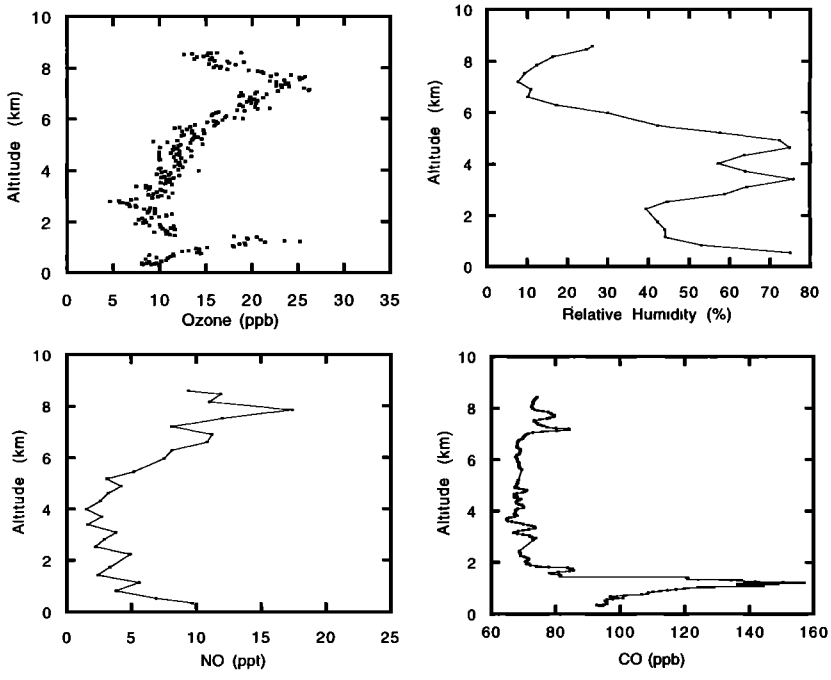

Figure 5. Vertical profiles of O_3, CO, NO, and relative humidity obtained in the tropical Pacific Ocean near 4.0°N, 124.8°E during PEM-West A mission 16 (October 13, 1991, 0330:30–0413:30 UT).

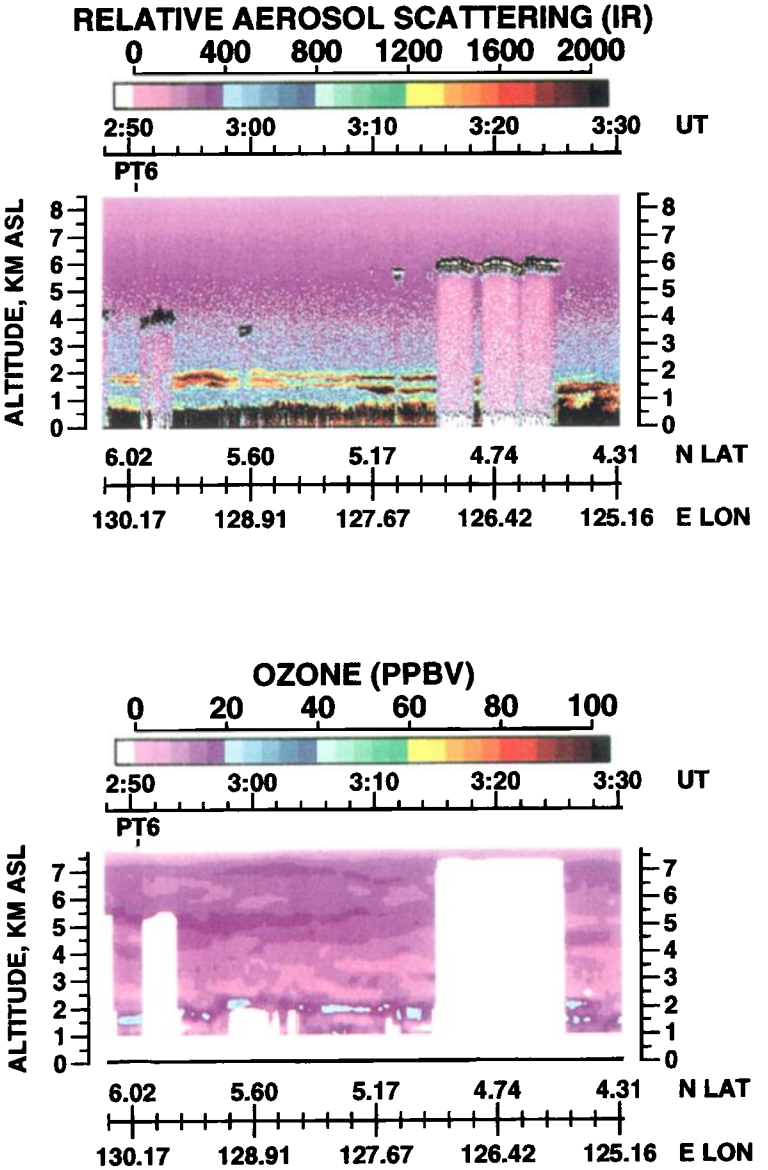

Figure 6. Vertical and horizontal distributions of (top) aerosol and (bottom) O_3 observed by downward looking DIAL during mission 16 (October 13, 1991) at 0250–0330 UT. Note the relatively high O_3 layer at 1.5–2.0 km that coincides with aerosol layer. Top of the mixing layer is indicated at 1.0 km.

Table 3. Daytime and Nighttime Gaseous and Particulate Cl Measured in the Marine Boundary Layer of the Tropical Pacific Ocean During PEM-West A

Mission	Time Period	Day/Night	Gaseous Cl, ppt	Aerosol Cl, ppt	Aerosol Na, ppt	Aerosol Ratio Cl/Na
17	1933:30–1951:00	night	25	310	273	1.14
	1952:00–2006:10	night	32	310	273	1.14
	0042:30–0100:00	day	49	230	221	1.04
	0101:00–0119:30	day	31	230	221	1.04
	0121:00–0128:00	day	38	230	221	1.04
20	1453:00–1506:30	night	111	166	198	0.84
	1507:00–1521:30	night	112	166	198	0.84
	1522:30–1534:00	night	123	166	198	0.84
	1817:30–1831:00	day	240	68	108	0.63
	1832:00–1846:00	day	156	68	108	0.63

Table 4. Estimates of Mean Net Entrainment Rates Across the Top of the Boundary Layer (BL) Required for Steady State

Mission	Measurement Period, UT	Free Troposphere O_3, ppb	BL O_3, ppb	BL Height, km	$P(O_3)$,* 10^5 molecules cm^{-3} s^{-1}	Entrainment Rate, V_e, mm s^{-1}
15	0330:30–0421:30	20	8.8	2.0	−3.2	3.9
16	0413:30–0454:30	12	8.4	0.8	−3.2	5.4
17	0050:30–0119:30	23	14.2	1.5	−3.2	3.8
18	0138:30–0212:30	26	8.5	1.2	−3.2	1.3

*Diurnally (24 hours) averaged. Negative $P(O_3)$ implies net photochemical ozone destruction.

average value obtained by *Kawa and Pearson* [1989] from 10 flights in the eastern Pacific Ocean in July and August 1985. Boundary layer heights were determined from the aircraft vertical temperature and humidity profiles and from the DIAL data. Frequently, the aerosol distribution data from the DIAL gave a better definition of the top of the marine boundary layer than the temperature/humidity profile (see, for example, Figure 6). The net photochemical tendency $P(O_3)$ was calculated from the model of *Davis et al.* [this issue] which is based on standard NO_x/HO_x chemistry:

$$P(O_3) = \{k_5[HO_2] + k_6[CH_3O_2] + k_7[RO_2]\}[NO] - k_4[H_2O][O^1D] - \{k_9[HO_2] + k_{10}[OH]\}[O_3] \quad (2)$$

The brackets indicate the concentration of a species and k_i values are the appropriate gas kinetic rate constants. In this model, $P(O_3)$ is described as the difference between the formation (first term) and the loss (second and third terms) rates of ozone. The basic input consists of fixed values for the mixing ratios of the observed chemicals O_3, NO, NO_2, H_2O, CO, and the physical parameters of temperature, pressure, and ultraviolet radiation flux. When $P(O_3)$ is positive, the net effect of tropospheric photochemistry is to provide a source of O_3; and when $P(O_3)$ is negative, it constitutes a net sink. Additional details can be found in the work of *Davis et al.* [this issue]. For missions 15–18 (Table 4) the photochemical destruction rates of ozone exceeded the formation rates. Mean (24 hours) formation and destruction rates of 2.4×10^5 and 5.6×10^5 molecules cm^{-3} s^{-1}, respectively, were calculated for the general conditions of missions 15–18. This corresponds to a 24-hour average net destruction rate of 3.2×10^5 molecules cm^{-3} s^{-1} (2.3 ppb d^{-1}). The net O_3 sink is the result of O_3 destruction by ultraviolet radiation in an extremely low NO environment (see Figures 2, 4, and 5) which prohibits significant ozone formation. As a rough measure, NO in excess of 10 ppt would be required before net O_3 production can occur. These estimates are within the range of previous estimates from the eastern Pacific by *Kawa and Pearson* [1989], who report a photochemical ozone sink of 3.0 ± 4.7 ppb d^{-1} in the summer.

Table 4 shows the values of net entrainment rate (V_e) computed from (1) together with the required input values. It is assumed that the mixing depth over the ocean did not change significantly during the course of a day. The calculated net entrainment rates vary from 1 to 5 mm s^{-1} with a mean value of 3.6 (±1.7) mm s^{-1}. This range of calculated net entrainment rates and its mean value are in good agreement with the range (1.0–5.0 mm s^{-1}) and mean value (3.0 ± 1.1 mm s^{-1}) reported by *Kawa and Pearson* [1989] from several aircraft flight measurements of O_3 and O_3 flux through the subsidence inversion that caps the marine boundary layer of the eastern Pacific Ocean. Our calculated values are also similar to the entrainment rates of 3.9 mm s^{-1} reported by *Paluch et al.* [1994] for the eastern Pacific Ocean.

An attempt was made to estimate entrainment rates by using water vapor as an independent tracer, recognizing at the outset that PEM-West A provided insufficient direct data for this purpose. The rate of evaporation for calm sea conditions, that generally prevailed for the periods of interest, was obtained from the technique presented by *Smith* [1988]. Data needed at the sea surface were available from either direct DC-8 measurements (e.g., seawater temperature from radiometry) or extrapolated from the data collected at flight level using standard assumptions (e.g., logarithmic wind velocity profile). For M15–M18, calculated evaporation rates varied from 0.4 to 1.9 $\times 10^{-6}$ g cm^{-2} s^{-1}. The entrainment rate across the top of the boundary layer (Table 4) required to balance the upward flux (evaporation) from the sea surface varied from 1.1 to 3.3 mm s^{-1} (2.1 ± 1.0 mm s^{-1}). It is noted that entrainment rate calculation for water vapor involves sensitive computations for which detailed data were not available. As an example, the calculated entrainment rates were higher by a factor of 1.8 when evaporation rates were calculated by the method of *Haltiner and Martin* [1957] instead of *Smith* [1988]. Ongoing analysis of data from the Central Equatorial Pacific Experiment (CEPEX) also appears to support these entrainment rates (R. Grossman, private communication, University of Colorado, 1994). Although net entrainment rates cannot be accurately calculated for this region, there appears to be sufficient indication that in the absence of convection (e.g., typhoons) these rates are in the vicinity of 1–5 mm s^{-1}. Thus it is likely that in the tropical and equatorial Pacific region, known photochemical and meteorological principles provide an adequate explanation of the observed low O_3 concentrations in the boundary layer.

Catalytic destruction of O_3 in the troposphere initiated by halogen free radicals (Cl, Br, I), following chemistry similar to that known for the stratosphere, has often been proposed (e.g., $Cl + O_3 \rightarrow ClO + O_2$; $ClO + HO_2 + h\nu \rightarrow HO + Cl + O_2$; $ClO + ClO \rightarrow Cl_2 + O_2$). Iodine and chlorine chemistry in marine air [*Chameides and Davis*, 1980; *Keene et al.*, 1990] and bromine chemistry in spring Arctic air [*Barrie et al.*, 1988] have all been suggested. Measurements of CH_3I in the marine troposphere clearly show that it is not sufficiently abundant to play an important role even if the proposed chemistry is correct. A difficulty with all these proposals is that halogen free radicals tend to quickly form relatively stable species (e.g., HCl, HI, HBr, HOBr) and in the absence of a mechanism for the rapid regeneration, significant free radicals concentrations cannot be sustained. *Keene et al.* [1990] have postulated that O_3 and OH

Table 5. Estimates of Cl Atom Concentrations in the Tropical Marine Boundary Layer

Chemicals	Rate Constants at 298 K,* cm^3 molecules^{-1} s^{-1}		Inferred Cl Atom Concentrations,† 10^5 molecules cm^{-3}	
	K_{OH}, $\times 10^{-12}$	K_{Cl}, $\times 10^{-10}$	Mission 17	Mission 20
Ethane	0.24	0.57	0.36	0.94
Propane	1.10	1.60	2.75	1.14
Acetylene	0.76	0.49	7.61	3.14
C_2Cl_4	0.17	0.41	2.12	3.98
DMS	4.90	3.30	0.18	...

*All OH as well as ethane and propane Cl rate constants are taken from *DeMore et al.* [1992]. Acetylene + Cl rate constant is the new recommended value in the W. B. DeMore et al. revision (unpublished, 1994). C_2Cl_4 + Cl rate is from *Atkinson and Aschmann* [1987] and P. Wine (private communication, GIT, 1994); and DMS + Cl rate is from *Stickel et al.* [1992].

†Equation (3) and data from Table 2 are used to derive Cl atom concentrations. OH concentrations of 3×10^6 molecules cm^{-3} are used. The time elapsed between the sunrise and the middle time of the measurements (Δt) was 2.2 hours for mission 17 and 1.9 hours for mission 20.

absorption to aerosols may release high concentrations of Cl atoms (1–5 $\times$ 10^6 molecules cm^{-3}) in the marine boundary layer and these may in some way catalytically destroy O_3 and be important sinks for organic species. They also predict high Cl_2 (4–8 ppb) concentrations at night and a pulse of HCl in the early morning.

Day-night measurements shown in Table 2 (missions 17 and 20) provided an opportunity to assess the presence of Cl atom concentrations in the early morning hours in an indirect way. As shown in Table 5, the reaction of Cl atoms with C_2H_6, C_3H_8, C_2H_2, C_2Cl_4, and dimethyl sulfide is extremely fast, and at 298 K, some 237, 145, 64, 241, and 67 times faster than their corresponding OH rate, respectively. These five chemicals were provisionally selected as the best potential indicators of Cl atom concentrations. It is reasonable to assume that DMS concentrations (and those of alkenes) were influenced by its proximate oceanic source, making it a less reliable molecule for this purpose. We assume that the source of the selected alkanes from seawater in this region is either nonexistent or extremely small [*Singh and Zimmerman*, 1992]. Measurable losses in C_2H_6 (1.3 to 2.5%), C_3H_8 (13–16%), C_2H_2 (12–28%) and C_2Cl_4 (9–12%) were seen over a 2-hour period after sunrise. Nighttime/daytime differences were normalized to CO concentrations, as it is expected to be inert over these timescales and can be used to normalize meteorological processes such as mixing. Cl atom concentrations ([Cl]) were calculated using (3).

$$[Cl] = \{\ln [([X]/[CO])_n/([X]/[CO])_m] - k_{OH}[OH]\Delta t\}/\{k_{Cl}\Delta t\} \quad (3)$$

where $([X]/[CO])_n$ and $([X]/[CO])_m$ are nighttime and morning (daytime) average mixing ratios of selected hydrocarbon and CO, k_{OH} and k_{Cl} indicate the rate constant of the appropriate hydrocarbon with OH and Cl, and Δt represents the elapsed sun-lit time (≈2 hours). Morning mean OH radical concentrations ([OH] = 2 to 3 $\times$ 10^6 molecules cm^{-3}) were estimated from the model described by *Davis et al.* [this issue] and this is generally a small quantity in (3). Table 5 summarizes the Cl atom concentrations as estimated with each of the organic molecules. Cl atom concentrations of 0.4–4.0 $\times$ 10^5 molecules cm^{-3} could be calculated from (3) when C_2H_6, C_3H_8, and C_2Cl_4 data are used. A similar calculation with C_2H_2 resulted in higher calculated Cl values (3–8 $\times$ 10^5 molecules cm^{-3}). Unlike the other species selected, C_2H_2 also reacts with Br atoms, but the rates are such ($k_{Cl}/k_{Br} \approx 550$) that this pathway would have a negligible effect unless large Br atom concentrations are present, which is considered unlikely. Mean Cl atom concentrations of 1.6 ± 1.4 $\times$ 10^5 molecules cm^{-3} (C_2H_2 results excluded) and 2.5 ± 2.3 $\times$ 10^5 molecules cm^{-3} (C_2H_2 results included) are calculated. It is noted that normalization by CO is not necessary and its exclusion changes these estimates only slightly (≈20%). It can be inferred (Table 5) that Cl atom concentrations were probably in the vicinity of 10^5 molecules cm^{-3}. If HCl (Table 3) was the main source of Cl atoms (HCl + OH → H_2O + Cl), then Cl atoms concentrations of only 10^2–10^3 molecules cm^{-3} could be sustained [*Singh and Kasting*, 1988]. Although these data show that marine boundary layer Cl atom concentrations are significantly below those proposed by *Keene et al.* [1990], the possibility that substantial concentrations (≈10^5 molecules cm^{-3}) still exist cannot be ruled out. A weakness of these indirect calculations is that extremely high precision and minimal atmospheric variability is implicit. Higher hydrocarbons (butanes and pentanes) could not be employed for these reasons.

Additional insight into the processes that may lead to Cl formation can be gained from the analysis of data in Table 3. First of all, gaseous Cl levels are relatively low at all times. There is no indication of extremely high Cl_2 (it is estimated that at least 50% of Cl_2 would be collected) concentrations or a large pulse of HCl in the morning hours, as proposed by *Keene et al.* [1990]. Night-day comparisons show that the Cl/Na ratio declines by about 10% during M17 and 25% during M20, indicating a substantial loss of aerosol chlorine. Coincident with this aerosol Cl loss, a gain in gaseous Cl was observed. This diurnal loss of Cl is intriguing, although similar behavior for Br has been previously reported [*Rancher and Kritz*, 1980]. Since acidification of marine aerosol is thought to be the principle mechanism for the release of gaseous Cl (thought to be largely HCl), this diurnal behavior may be attributed to the rapid formation of HNO_3 or H_2SO_4. However, available NO_x and SO_2 data do not support rapid acid formation. This would be consistent with the view that mechanisms other than acidic displacement are responsible for Cl atom concentrations of ≈10^5 molecules cm^{-3} in the marine boundary layer.

Conflicting reports based on aerosol chamber studies have suggested that molecular chlorine (Cl_2) may be a product of reactions involving sea-salt aerosols, O_3, and sunlight [*Zetzsch et al.*, 1988; *Zetzsch and Behnke*, 1992]. Preliminary measurements have been made to suggest that some forms of active chlorine [*Pszenny et al.*, 1993] and even Cl_2 (C. Spicer, private communication, 1992) may be present in the marine boundary layer. The concept of photoconversion of halogen ions (X^- = Cl^-, Br^-) to active halogen gas been around for decades [e.g., *Duce et al.*, 1965; *McConnell et al.*, 1992].

$$4X^- + O_2 + 4H^+ + h\nu \rightarrow 2\ X_2 + 2\ H_2O$$

The details of the above reaction sequence are not well known but may involve reaction with H_2O_2 (H_2O_2 (aq) + $2Cl^- \rightarrow Cl_2$ + 2 OH^-) or transitional metal ions (M^{n+} Cl + $h\nu \rightarrow$ $M^{(n-1)+}$ + Cl; Cl + Cl → Cl_2). Other possibilities involving reactions with NO_2 (Cl^- + $2NO_2$ (aq) → NOCl + NO_3^-;

$NOCl + h\nu \rightarrow NO + Cl$) or N_2O_5 ($Cl^- + N_2O_5\ (aq) \rightarrow ClNO_2 + NO_3^-$; $ClNO_2 + h\nu \rightarrow NO_2 + Cl$) are highly unlikely to be effective in the low NO_x environment of the tropical boundary layer. Some of the possible mechanisms that may cause active chlorine to be released from sea-salt aerosol have been reviewed by *Finlayson-Pitts* [1993].

Cl atoms can alter both the rates of formation and the destruction of O_3. Under extremely low NO conditions, as were present in the tropical marine boundary layer, Cl atoms can potentially destroy O_3. Photochemical calculations with the *Singh and Kasting* [1988] model and the Harvard box model (D. Jacob, private communication, Harvard University, 1994) suggest that Cl atoms in the vicinity of 10^5 molecules cm^{-3} can only cause a slight net rate of O_3 destruction ($\approx$0.1 ppb d^{-1}). This is negligible (<5%) in comparison with the net O_3 loss resulting from the NO_x/HO_x chemistry (Table 4). The effect of Cl chemistry on O_3 loss becomes significant at 10^6 molecules cm^{-3} Cl ($\approx$2 ppb d^{-1}). We also note that the mechanisms that may release Cl_2 (or HOCl) from sea salt would likely also release Br_2 (or HOBr), and Br atoms may be more effective in O_3 destruction. However, given the low total bromine availability in the marine aerosol [*Singh*, 1995], Br atom abundance is expected to be very low ($\ll 10^4$ molecules cm^{-3}). This is very much unlike the high Arctic spring environment where Br atoms in the range of 10^7–10^8 molecules cm^{-3} have been inferred to be present for relatively short periods of time [*Jobson et al.*, 1994]. Thus it appears that fast halogen chemistry probably occurs but is not likely to be a major factor behind these observed low tropical O_3 concentrations.

4. Conclusions

PEM-West A measurements in the tropical Pacific Ocean during October 1991 confirm the existence of an ozone minimum in the remote marine boundary layer. It is also shown that layers of high concentration ozone from the upper tropospheric ozone-rich air are often trapped in the tropical and equatorial boundary layer in that region. Model computations suggest that the low ozone concentrations in the remote marine boundary layer of the tropical Pacific Ocean are the result of photochemical destruction in a low nitric oxide environment, sea surface deposition, and relatively low net entrainment rates from the free troposphere. Although substantial chlorine atom concentrations may exist in the tropical marine boundary layer, halogen-initiated photochemistry is not likely to be a major factor in creating the observed low ozone concentrations.

Acknowledgments. This research was supported by the NASA Global Tropospheric Experiment. We acknowledge all PEM-West A participants for their cooperation and support. Special thanks are due to the flight and ground crew of the NASA Ames Research Center for making this effort a success. We are grateful to W. Viezee of SRI International and to H. Lee and E. Shadd of Synernet for meteorological and computational assistance. Constructive discussions with D. Jacob of Harvard University, D. Lenschow of the National Center for Atmospheric Research, R. Grossman of the University of Colorado, and R. Chatfield of NASA Ames are much appreciated.

References

Atkinson, R., and S. M. Aschmann, Kinetics of the gas phase reaction of Cl atoms with chloroethenes at 298 ± 2 K and atmospheric pressure, *Int. J. Chem. Kinet.*, *19*, 1097–1105, 1987.

Bachmeier, S., R. E. Newell, M. C. Shipham, Y. Zhu, D. R. Blake, and E. V. Browell, PEM-West A: Meteorological overview, *J. Geophys. Res.*, this issue.

Barrie, L. A., J. W. Bottenheim, R. C. Shnell, P. J. Crutzen, and R. A. Rasmussen, Ozone destruction and photochemical reactions at polar sunrise in the lower arctic atmosphere, *Nature*, *334*, 138–140, 1988.

Browell, E. V., et al., Large-scale air mass characteristics observed over the western Pacific during the summertime, *J. Geophys. Res.*, this issue.

Chameides, W. L., and D. D. Davis, Iodine: Its possible role in tropospheric photochemistry, *J. Geophys. Res.*, *85*, 7383–7398, 1980.

Davis, D. D., et al., An assessment of ozone photochemistry in the western North Pacific as inferred from PEM-West A observations during fall 1991, *J. Geophys. Res.*, this issue.

DeMore, W. B., S. P. Sander, D. Golden, R. F. Hampson, M. J. Kurylo, C. J. Howard, A. R. Ravishankara, C. E. Kolb, and M. J. Molina, Chemical kinetics and photochemical data for use in stratospheric modelling, in *Evaluation 10, JPL Publ. 92-20*, Jet Propul. Lab., Pasadena, Calif., 1992.

Duce, R. A., J. W. Winchester, and T. W. Van Nahl, Iodine, bromine and chlorine in the Hawaiian marine atmosphere, *J. Geophys. Res.*, *70*, 1775–1799, 1965.

Finlayson-Pitts, B. J., Chlorine atoms as potential tropospheric oxidant in marine boundary layer, *Res. Chem. Intermed.*, *19*, 235–249, 1993.

Fishman, J., et al., Vertical profiles of ozone, carbon monoxide, and dew point temperature obtained during GTE/CITE 1, October–November 1983, *J. Geophys. Res.*, *92*, 2083–2094, 1987.

Haltiner, G. J., and F. L. Martin, *Dynamical and Physical Meteorology*, 470 pp., McGraw Hill, New York, 1957.

Hoell, J. M., D. D. Davis, S. C. Liu, R. Newell, M. Shipham, H. Akimoto, R. J. McNeal, and R. J. Bendura, Pacific Exploratory Mission-West A (PEM-West A): September–October 1991, *J. Geophys. Res.*, this issue.

Jobson, B. T., et al., Measurements of C_2-C_6 hydrocarbons in the high Arctic: Evidence for Br and Cl chemistry during low ozone episodes at Alert, *J. Geophys. Res.*, *99*, 25,355–25,368, 1994.

Kawa, S. R., and R. Pearson Jr., Ozone budgets from the Dynamics and Chemistry of Marine Stratocumulus Experiment, *J. Geophys. Res.*, *94*, 9809–9817, 1989.

Keene, W. C., A. A. P. Pszenny, R. A. Duce, D. J. Jacob, J. N. Galloway, J. J. Schultz-Tokos, H. Sievering, and J. F. Boatman, The geochemical cycling of reactive chlorine through the marine troposphere, *Global Biogeochem. Cycles*, *4*, 407–430, 1990.

Liu, S. C., M. McFarland, D. Kley, O. Zafiriou, and B. Huebert, Tropospheric NO_x and O_3 budgets in the equatorial Pacific, *J. Geophys. Res.*, *88*, 1360–1368, 1983.

McConnell, J. C., G. S. Henderson, L. Barrie, J. Bottenheim, H. Niki, C. H. Langford, and E. Templeton, Photochemical bromine production implicated in arctic boundary-layer ozone depletion, *Nature*, *355*, 150–152, 1992.

Merrill, J. T., Trajectory results and interpretation for PEM-West A, *J. Geophys. Res.*, this issue.

Newell, R. E., and M. F. Wu, Simultaneous measurements of carbon monoxide and ozone in the NASA Global Atmospheric Sampling Program (GASP), in *Atmospheric Ozone*, edited by C. S. Zerefos and A. Ghazi, pp. 548–552, D. Reidel, Norwell, Mass., 1985.

Paluch, I. R., D. H. Lenschow, S. Siems, G. L. Kok, and R. D. Schillawski, Evolution of the subtropical marine boundary layer, I, Comparison of soundings over the eastern Pacific from FIRE and HaRP, *J. Atmos. Sci.*, *51*, 1465–1479, 1994.

Piotrowicz, S. R., D. A. Boran, and C. J. Fisher, Ozone in the boundary layer of the equatorial Pacific Ocean, *J. Geophys. Res.*, *91*, 13,113–13,119, 1986.

Piotrowicz, S. R., H. F. Bezdek, G. R. Harvey, and M. Springer-Young, On the ozone minimum over the equatorial Pacific Ocean, *J. Geophys. Res.*, *96*, 18,679–18,687, 1991.

Pszenny, A. P., W. C. Keene, D. J. Jacob, S. Fan, J. R. Maben, M. P. Zetwo, M. Young-Springer, and J. N. Galloway, Evidence of inorganic chlorine gases other than hydrogen chloride in marine surface air, *Geophys. Res. Lett.*, *20*, 699–702, 1993.

Rancher, J., and M. A. Kritz, Diurnal fluctuations of Br and I in the tropical marine atmosphere, *J. Geophys. Res.*, *192*, 5581–5587, 1980.

Routhier, F., R. Dennett, D. D. Davis, A. Wartburg, P. Haagenson, and A. C. Delany, Free tropospheric and boundary layer airborne measurements of ozone over the latitude range of 58°S and 70°N, *J. Geophys. Res.*, *85*, 7307–7321, 1980.

Singh, H. B., Halogens in the atmospheric environment, in *Composition, Chemistry and Climate of the Atmosphere*, edited by H. B. Singh, VNR, New York, 1995.

Singh, H. B., and J. F. Kasting, Chlorine-hydrocarbon photochemistry in the marine troposphere and lower stratosphere, *J. Atmos. Res.*, *7*, 261–285, 1988.

Singh, H. B., and P. Zimmerman, Atmospheric distributions and sources of nonmethane hydrocarbons, *Adv. Environ. Sci. Technol.*, *24*, 177–235, John Wiley, New York, 1992.

Singh, H. B., W. Viezee, and L. J. Salas, Measurements of selected C_2-C_5 hydrocarbons in the troposphere: Latitudinal, vertical, and temporal variations, *J. Geophys. Res.*, *93*, 5861–5878, 1988.

Singh, H. B., et al., Summertime distribution of PAN and other reactive nitrogen species in the northern high-latitude atmosphere of eastern Canada, *J. Geophys. Res.*, *99*, 1821–1835, 1994.

Smith, S. D., Coefficients for sea surface wind stress, heat flux, and wind profiles as a function of wind speed and temperature, *J. Geophys. Res.*, *93*, 15,467–15,472, 1988.

Stickel, R. E., J. M. Nicovich, S. Wang, Z. Zhao, and P. H. Wine, Kinetic and mechanistic study of the reaction of atomic chlorine with dimethyl sulfide, *J. Phys. Chem.*, *96*, 9875–9883, 1992.

Talbot, R. W., A. S. Vijgen, and R. C. Harriss, Measuring tropospheric HNO_3: Problems and prospects for nylon filter and mist chamber techniques, *J. Geophys. Res.*, *95*, 7553–7561, 1990.

Zetzsch, C., and W. Behnke, Heterogeneous sources of atomic Cl in the troposphere, *Ber. Bunsenges. Phys. Chem.*, *96*, 488–493, 1992.

Zetzsch, C., G. Pfahler, and W. Behnke, Heterogeneous formation of chlorine atoms from NaCl in a photosmog system, *J. Aerosol. Sci.*, *19*, 1203–1206, 1988.

B. Anderson, E. Browell, G. L. Gregory, and G. W. Sachse, NASA Langley Research Center, Hampton, VA 23665.

D. R. Blake, University of California, Irvine, CA 92717.

J. D. Bradshaw, J. C. Crawford, and D. D. Davis, Georgia Institute of Technology, Atlanta, GA 30332.

J. Merrill, University of Rhode Island, Narragansett, RI 02882.

R. Newell, MIT, Cambridge, MA 02139.

H. B. Singh (corresponding author), NASA Ames Research Center, Stop 245-5, Moffett Field, CA 94035.

R. Talbot, University of New Hampshire, Durham, NH 03824.

D. Thornton, Drexel University, PA 19104.

(Received May 13, 1994; revised February 20, 1995; accepted February 20, 1995.)